



# Novel projection welding technology for joining of steel-aluminum hybrid components—part 1: technology and its potential for industrial use

Anastasiia Zvorykina<sup>1</sup> · Oleksii Sherepenko<sup>1</sup> · Sven Jüttner<sup>1</sup>

Received: 28 August 2019 / Accepted: 18 November 2019 / Published online: 9 December 2019  
© International Institute of Welding 2019

## Abstract

Multi-material design offers cost-efficient lightweight solutions for automotive body-in-white production. Ultra-high strength steels remain an essential part of the lightweight construction and are increasingly used in combination with components made of aluminum alloys in multi-material body designs. For these applications, the commonly used joining processes (riveting, clinching, resistance spot welding, etc.) have been pushed to their technological limits and a further technological development is needed. The present research describes a new joining technology based on resistance welding process for joining ultra-high strength steel 22MnB5 (AS150) with aluminum sheets AW 6016. The technology consists of a two-stage resistance spot welding process with an additional simple cost-effective joining element. Its implementation allows joining aluminum and steel on extremely short flanges of 10 mm using short time projection welding with high-energy concentration. Joining elements—cylinders made of Cu- and Fe-based wires with diameter 1.6 mm and length 10 mm - were welded using the common resistance spot welding equipment. Experimental results have shown that all tested materials for joining dissimilar steel-aluminum compounds can be successfully used and the weld current ranges are sufficient for industrial application.

**Keywords** Joining technology · Resistance spot welding · Projection welding · Multi-material design · Dissimilar materials · Aluminum to steel · 22MnB5 · Ultra-high strength steel

## 1 Introduction

Current multi-material lightweight design strategy in automotive body in white involves production of dissimilar joints between steel and low-density alloys as aluminum; therefore, a large amount of research has been conducted in this area over the past

years [1–6]. Difficulties with thermal joining of these materials are caused by differences in thermo-physical properties, especially thermal expansion, thermal conductivity, as well as melting points (~660 °C for Al alloy and ~1497 °C for steel). Another challenge is nearly zero solid solubility of iron in aluminum and the formation of brittle intermetallic compounds, leading to the reduction of mechanical properties of the joints [2].

Several methods are commonly used to manufacture aluminum-steel joints in the automotive production, for instance mechanical joining technologies like self-piercing riveting, screwing, and clinching have a good potential for Al to steel joining and are often combined with adhesive bonding [3, 7]; however, their cost-effective use for ultra-high strength or low ductile boron steels is limited [4]. Resistance spot welding has been investigated in several studies [5, 6]. It was used to produce aluminum to steel joints of Zn-coated steels, alternatively, additional Zn-inserts were used [8, 9].

For new lightweight construction, in particular combinations of ultra-high-strength materials with dissimilar materials, the commonly used processes have been

---

Recommended for publication by Commission III - Resistance Welding, Solid State Welding, and Allied Joining Process

---

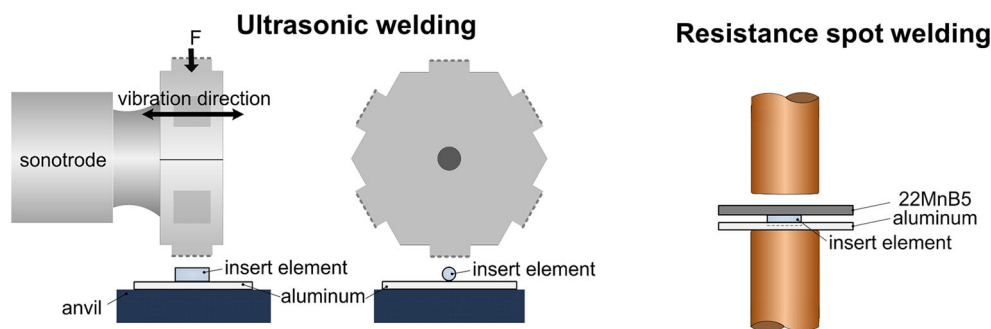
✉ Anastasiia Zvorykina  
anastasiia.zvorykina@ovgu.de

Oleksii Sherepenko  
oleksii.sherepenko@ovgu.de

Sven Jüttner  
sven.juettner@ovgu.de

<sup>1</sup> Institute of Materials and Joining Technology (IWF), Otto von Guericke University Magdeburg, Universitätsplatz 2, 39106 Magdeburg, Germany

**Fig. 1** Ultrasonic resistance spot welding processes using cylinder insert element made of steel (after [11])



pushed to their technological limits. One of the approaches to extend these boundaries is the use of hybrid joining technologies with an additional element. For instance, resistance element welding (REW) has been suggested lately [4]. Depending on the joined materials, several variations of this process exist, all of them involving two process stages. If one of the joint partners is soft and is accessible, the element can be inserted through it and a subsequent resistance weld can be made. Otherwise, extra pre-punching of holes is needed, increasing production costs [4].

Another method for element application is ultrasonic welding, which is followed by resistance welding in the second process stage, whereas no penetration from the outside is needed. Several investigations of a combined USW + RP welding process can be found in the literature [10–12]. Zvorykina et al. [11] use a steel insert element (see Fig. 1), Lu et al. [12] suggest the use of an aluminum insert element. However, industrial use of these processes is limited due to strong wear of a sonotrode. Because of large contact surface between insert element and steel or aluminum, long welding times are used in the resistance welding process, leading to high heat input, causing problems when combining welding and adhesive

bonding [13]. This issue can be solved by welding with short welding times and high currents, combined with a small joint contact surface increasing the energy concentration and thus reducing the heat input in the HAZ, so that the adhesive damage is minimized, as reported by Holtschke et al. [14].

### 1.1 Novel resistance spot welding technology for joining of hybrid components

The new joining technology is based on a two-stage welding process: the joints are made by using a single conventional resistance spot welding machine and the insert elements are made from conventional filler wire. This allows an extremely cost-effective manufacturing of insert elements. Their dimensions and chemical composition can be simply modified.

The process, shown in Fig. 2, consists of two stages. In the first stage, an insert element is joined with an aluminum sheet by a projection welding process. In the second stage, the aluminum sheet (together with the welded insert element) is joined with a steel sheet, resulting in both sheets held together by the insert element. Process options include use of adhesive after the first stage for welding steel and aluminum by an insert element.

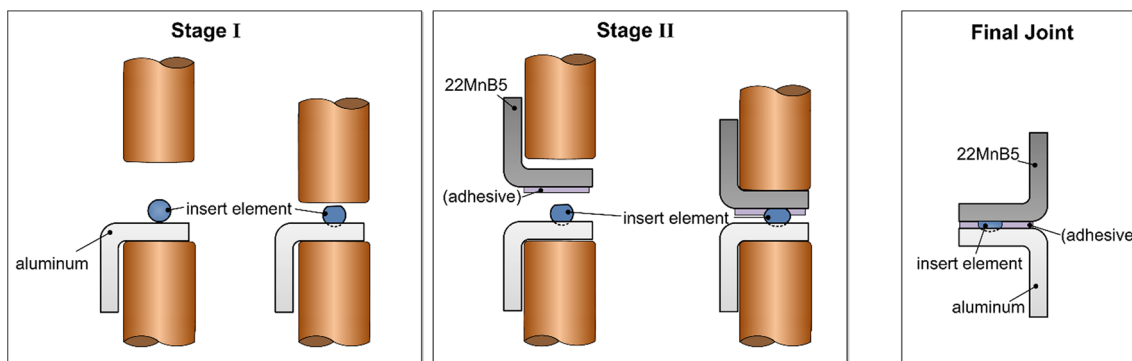


**Fig. 2** Two stages of a hybrid projection welding process with the insert element: (1) securing of element on aluminum sheet; (2) application of adhesive, if required; and (3) manufacturing of entire joint

**Table 1** Chemical composition of sheet metals (in wt%)

	C	Mn	P	S	Si	Al	Ti	B
22MnB5 + AS150	0.23	1.18	0.0109	0.0008	0.254	0.04	0.04	0.0032
	Cr	Mn	Cu	Mg	Si	Al	Ti	Fe
EN AW 6016	0.18	0.13	0.07	0.39	1.27	Balance	0.03	0.26

The applied joining process can be categorized as projection welding, since, due to the use of cylindrical insert elements, linear contact between the sheet and the element with a relatively small contact surface is formed, so that current flow is not determined by the geometry of the electrode but by the shape of joining parts. The use of a cylindrical insert element made of wire ensures small contact surface and enables welding with welding times of several milliseconds, resulting in an extreme low total heat input, so that in case of a hybrid joining process, where adhesive is applied after the first step, it is not thermally damaged, opposite to conventional resistance welding. Additionally, the heat-affected zone (HAZ) is very small, which may be advantageous when welding high strength steel. Because of using flat electrode tips for the projection welding process allows manufacturing welded joints without visible electrode indentation, so it is perfectly suited for applications where no visible welds can be tolerated.

The geometry of the welded joint can be easily controlled by adjusting element geometry and welding parameters. Depending on the dimensions and position of the insert elements, it is possible to weld very close to the edge of the aluminum sheet, e.g., in case of short-flange joints. By changing the diameter of the element, the gap between the sheets can be adjusted and controlled. This plays an important role in the manufacturing of hybrid joints with adhesive, because the thickness of adhesive layer influences the final tensile strength [15].

As the process consists of two stages, making the weld at the precise position where the element was placed in the first process step might be an issue during industrial application. It is to be addressed in further studies.

The current paper presents an example of applying the novel projection welding technology with insert elements for producing hybrid aluminum-steel joints with a possibility to a combination of projection welding and adhesive bonding. Effects of welding parameters and chemical composition of the insert element on the process window are discussed.

## 2 Experimental

### 2.1 Test materials and experimental procedure

The joining of aluminum to steel was conducted on 1.0mm thick EN AW 6016-T4 alloy sheets and 1.5-mm-thick boron steel 22MnB5 with Al-Si coating of 150 g/m<sup>2</sup>, press hardened at 930 °C for 6 min. The steel sheets with dimensions of 300 × 490 mm where cleaned with alcohol, placed into a furnace, which was preheated to a chosen temperature. After the holding time, the sheets were rapidly transported into a flat die and cooled with a cooling rate higher than 27 °C/s and a compression force of 70 kN. The chemical composition of test materials is provided in Table 1. The microstructure of test materials prior to welding is shown in Fig. 3.

Cylinder insert elements (IE) made of Cu- and Fe-based wires with a diameter of 1.6 mm were used. All elements were manually cut to a length of 10 mm. The chemical composition of the used materials is shown in Table 2.

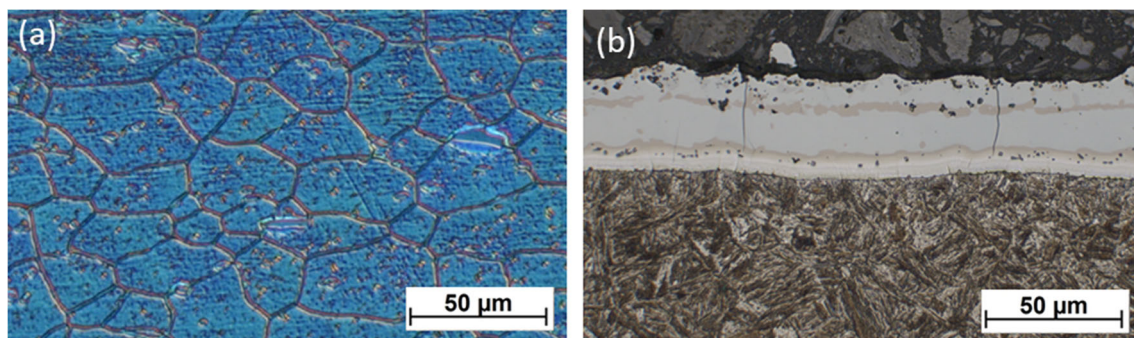


**Fig. 3** Microstructure of sheet materials prior to welding. **a** Aluminum EN AW 6016 (etched with Weck color etching). **b** 22MnB5 with Layer of AS150 after press hardening (nital-etched)

**Table 2** Chemical compositions of wires for insert elements (in wt%)

	C	Si	Mn	Cr	Mo	Ni	Sn	Cu	Nb	Fe
Cu-based	–	0.28	0.27	–	–	< 0.005	4.97	Balance	–	< 0.005
CrNi-steel	0.02	0.88	1.84	20.0	0.11	9.95	0.01	0.1	0.01	Balance

## 2.2 Welding and testing procedure

Welding was performed, using a stationary welding system in C-construction with a 1000 Hz medium frequency (MFDC) inverter from Nimak with a magnetic force control unit “magneticDrive.” The force during the welding process is applied, using an electromagnet, and is being held constant during the welding process, as described in detail in [16]. All welds were made with flat electrode tips C0 according to DIN EN ISO 5821:2010-04 made of CuCr1Zr alloy with diameter of 16 mm. Welding current, voltage drop between the electrodes, electrode force and displacement were monitored for each weld, using an HKS WeldQAS measuring device with a measurement frequency of 256 kHz.

By combination of high welding current with extremely high current ramping (between 3 and 12 kA/ms for the investigated insert elements and sheet combinations) and small contact surface between metal sheet and the insert element, a

very high current flux density through the contact surface in the joint plane can be achieved. Supported by the magnetic follow-up unit, this allows using extremely short, as for MFDC, welding times between 10 and 50 ms.

Figure 4 shows typical measured process variable electrode force, welding current, and electrode displacement, for stage II when welding with a copper insert element with a welding time of 10 ms and welding current of 27 kA. The magnified view (Fig. 4b) shows, that deformation of the welded joint takes place (as can be seen from the electrode displacement) after the welding current is ceased. This corresponds to the observations of Rusch and Stocks [17] for capacitor discharge welding, which is also characterized by an extremely high energy concentration. For the investigated joining process, it may be suggested that surface activation due to metal vaporization takes place during the current flow, followed by contacting of the activated surfaces, so that the joining is formed with little to no liquid phase involved. As a result no weld nugget is formed as described in [18].

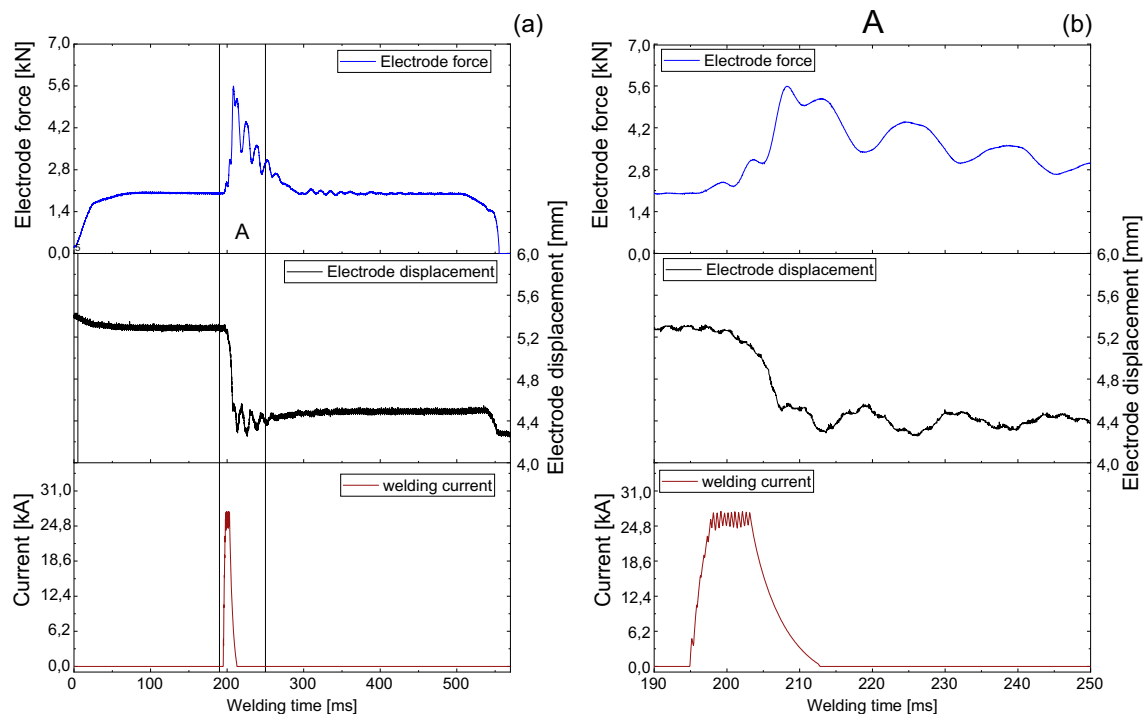


**Fig. 4** Measured welding current, electrode force, and displacement in the welding process for stage II when welding with a copper insert element. Welding time 10 ms, welding current of 27 kA. **a** General view. **b** Magnified view

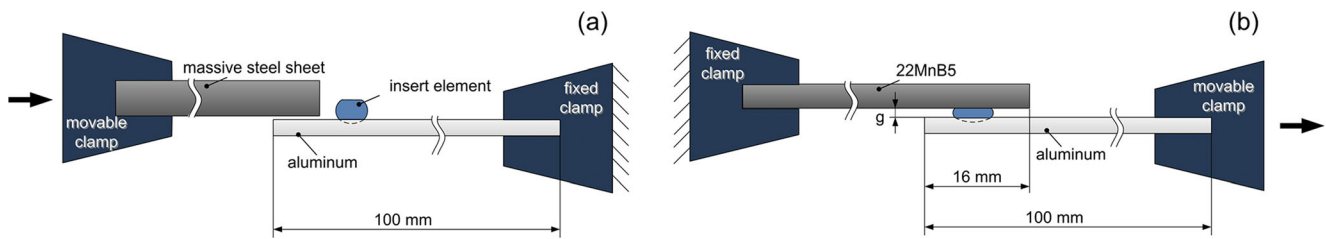


**Fig. 5** Determination of mechanical properties of joints after processing stages I and II. Stage I, shear off test of the insert element; stage II, lap shear test for determination of lower boundary of WCR

As the joint is formed without a weld nugget, determination of welding current ranges (WCR) based on common guidelines, where the lower WCR is defined by nugget diameter, like SEP 1220-2 [19], is not applicable. Moreover, as the investigated welding process incorporates two stages, assessment of welding parameters must be done for the first stage, prior to determining the parameters for the second one.

Although DVS 2911 [20] suggests a method of the lower WCR boundary determination by metallographic investigations, measuring the joint length, no data could be found in the literature, showing the correlation between bonded length and mechanical properties of the welded joint. The definition of the upper WCR boundary, based on expulsion classification proposed by Ketzel et al. [18], is subjective and has been developed for massive projection joints, making its direct application for welding of small functional elements difficult.

Mechanical properties were used to determine the lower boundary of WCR for both process stages, as shown in Fig. 5. For the first stage, instrumented shear off test of the element was conducted. The insert element was welded on a  $100 \times 35$ -mm aluminum sheet, so that the element longest axis was 10 mm from the sheet edge. The element was then sheared off with a massive steel plate. The maximum force, at which the element was sheared off from the aluminum plate ( $F_S$ ), was documented. The element was considered reliably joined with the aluminum sheet, if the  $F_S$  was larger or equal to 100 N. Starting with the welding current of 5 kA for steel element and 10 kA for copper element, 3 welds per welding current setting were made and tested. If the shear off force

for at least one specimen was lower than 100 N, the welding current was increased by 1 kA and three new weld joints were produced and tested. Due to a large parameter window, the welding current was increased by 1 kA, instead of more typical 200 A. This was repeated until  $F_S$  for all three specimens was larger than 100 N. This current setting was defined as the lower WCR boundary  $I_{\min}$ .

For the second stage, a lap shear test using the same specimen geometry with a reduced overlap of 16 mm (as in [4]) was employed. The variation of welding current was made as described for the first stage, the starting welding current was set to 10 kA for the steel insert element and to 14 kA for the copper insert element. The minimum lap shear strength for defining the lower WCR boundary was set to 1 kN.

After definition of the lower WCR boundary, welding current was further increased in steps of 1 kA until the upper WCR boundary was reached. For that purpose, specimens with dimensions of  $35 \times 35$  mm were used. The insert element geometry was not altered.

For the first stage, the upper WCR boundary was defined by maximum deformation of the insert element and its indentation into aluminum as shown in Fig. 6. For the second process stage, a gap between steel and aluminum sheet was used for that purpose.

To define the joint deformation  $D$ , two specimens with the same welding current were made. Subsequently, the joint height  $h_1$  was measured on the three specimens—in the middle and 3 mm left and right from the element center using a vernier caliper, then a joint height  $h_1$  was calculated as a mean of all three measurements and the total joint deformation ( $D$ ) was calculated for each of two investigated specimens, using Eq. (1), where  $h$  is a known height of the welded joint,

**Fig. 6** Definition of upper WCR boundary for steps I and II of the joining process

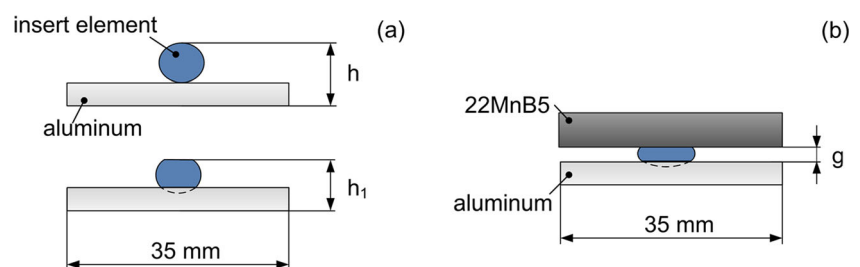


**Table 3** Parameter variation for the WCR determination in stage I and stage II of the welding process

Stage I			Stage II		
Electrode force	Welding time	Boundary	Boundary of stage I (10 ms)	Welding time	Electrode force
2 kN	10 ms	I <sub>min</sub>	I <sub>min</sub>	10 ms	4 kN
		I <sub>max</sub>		16 ms	
	16 ms	I <sub>min</sub>	I <sub>max</sub>	10 ms	
		I <sub>max</sub>		16 ms	

resulting from sheet thickness of 1.0 mm and element diameter of 1.6 mm (2.6 mm). Based on previous empirical observations, the deformation of the element in the first process stage did not to exceed 40%. The highest welding current setting, for which this condition was filled for both welded specimens, was determined as the upper boundary of the WCR  $I_{\max}$ .

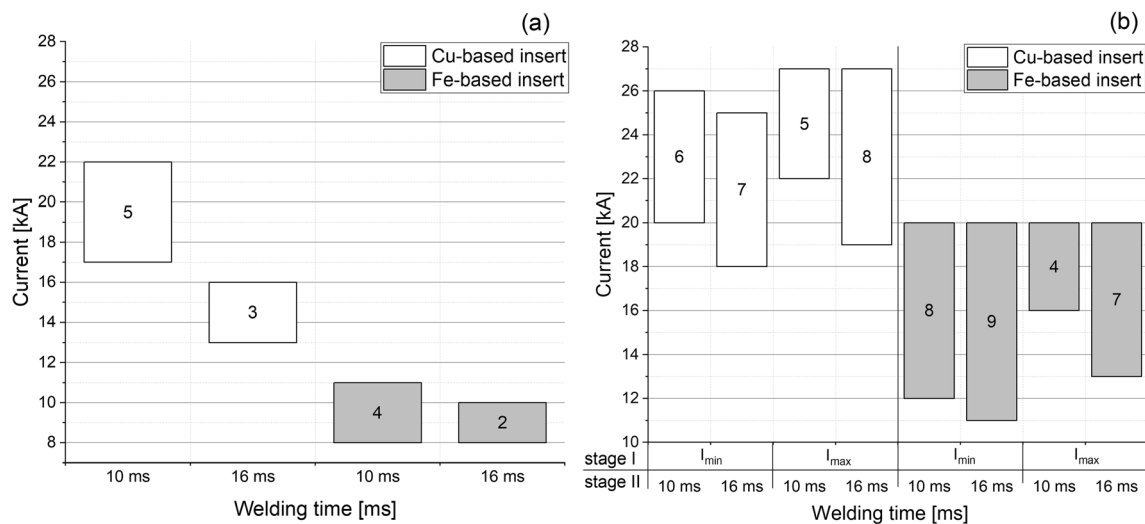
For the second stage, the same specimen geometry and quantity as well as procedure of the upper WCR boundary determination was used, but the gap between the joined sheets ( $g$ ) was used as a criterion for the boundary definition. The gap, shown in Fig. 6, was measured using a gauge. The measurement was conducted on both sides of the insert element, parallel to its longer side and then the mean of both measurements ( $g$ ) was calculated for each specimen. The highest welding current, for which the mean gap height ( $g$ ) for both specimens was not lower than 0.1 mm and no visible destruction of the insert element was detected, was determined as the upper boundary of the WCR  $I_{\max}$ .

$$D = \frac{h-h_1}{h} \cdot 100\% \quad (1)$$

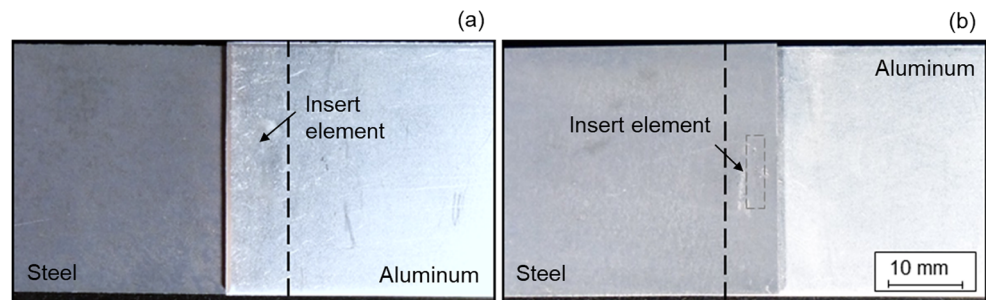
First, the welding current ranges for the first stage, using welding times of 10 and 16 ms were determined for both insert elements. To show the influence of welding parameters of the first stage on the second stage of the welding process, specimens at the boundaries of WCR for the welding time of 10 ms were welded and used to determine WCRs in the process stage II. This was also conducted for both insert elements, resulting in overall 2 WCRs per element for the first process stage and 4 WCRs per element for the second process stage, as shown in Table 3.

For metallographic examinations, cross sections for  $I_{\min}$  and  $I_{\max}$  were prepared using standard procedure: subsequently grinded and polished. The small samples (with dimensions 35 mm × 35 mm) were prepared and a cross section specimen was extracted out in the middle of the insert element, transverse to its longer side with a laboratory wet abrasive cutter.

To determine the influence of the heat-affected zone in the high strength steel sheet on its properties, cross sections were additionally etched according to recommendations of DVS 2916-4 with nital etching. Besides that, the tensile shear test was made to determine the influence of heat input on specimen strength. The small aluminum samples with dimensions of 35 mm × 35 mm were welded on the samples made of steel sheets with dimensions of 235 mm × 25 mm using insert

**Fig. 7** Experimentally obtained welding current ranges. **a** For stage I. **b** For stage II

**Fig. 8** A top view of the joint after stage II **a** from aluminum side (without mark) and **b** steel side (marked) with the 6 mm flange length welded by using Fe-based IE with 4 kN welding force, 16 ms welding time, 20 kA welding current



elements. For comparison, steel samples without a weld with dimensions of 235 mm × 25 mm were used.

### 3 Results and discussion

As expected, much higher welding currents were needed to join more conductive copper-based elements, compared with more resistive steel elements (electrical resistivity for Cu-IE  $1.25\text{--}1.35 \cdot 10^{-7} \Omega \text{ m}$  and for Fe-IE  $7.3 \cdot 10^{-7} \Omega \text{ m}$ ). As seen in Fig. 7 a, the resulting weldability lobes for stage I for Cu-based and Fe-based insert elements respectively show large differences, depending on welding current and welding time. It can be seen that for Cu-based elements, the weldability lobes shift to lower welding currents with increasing welding time and the size of the WCR decreases. For Fe-based elements, no such strong shift of WCR is observed; however, the upper WCR boundary is shifted to lower welding current by 1 kA when increasing welding time from 10 to 16 ms. It can be assumed that the narrowing of the WCRs is caused by longer welding time, higher heat input, and therefore stronger deformation of the element. Due to wider size of the weldability lobes for both elements, shorter welding time of 10 ms is more suitable for further use.

The welding current ranges shown in Fig. 7 b were obtained for both insert element materials for stage II. The size of the weldability lobes varies insignificantly between 5 and 8 kA. Only the size of the welding current range with the welding time on the stage II of 10 ms for the Fe-based insert element drops down to 4 kA. Caused by low electrical resistance of copper elements, higher welding currents were needed to join steel and aluminum with copper insert elements, corresponding to the observations, made in stage I. From an industrial point of view, the larger the welding current range, the better process stability can be achieved. Due to that, big size of the weldability lobes is advantageous and 16 ms welding time for stage II should be used for further investigations.

Top view of an entire steel-aluminum joint is shown in Fig. 8 a view from steel side as well as Fig. 8 b from aluminum side. Due to the fact that no visible electrode indentation can be seen, the joining point is hard to recognize from the outside. Furthermore, the possibility for shortening the flange length up to 6 mm can be seen. Insert element can be positioned very close to the edge of the aluminum sheet and to the steel sheet respectively.

For joints welded with  $I_{\min}$  and  $I_{\max}$  on the stage I, images of cross sections were made. Figure 9 shows a cross section micrograph of the elements after stage I welded at the lower

**Fig. 9** Cross sections of Cu-based and Fe-based insert elements (IE) welded on aluminum sheet on the stage I with 2 kN welding force and 10 ms welding time with **a, c** lower limit for welding current ( $I_{\min}$ ) and **b, d** upper limit for welding current ( $I_{\max}$ )

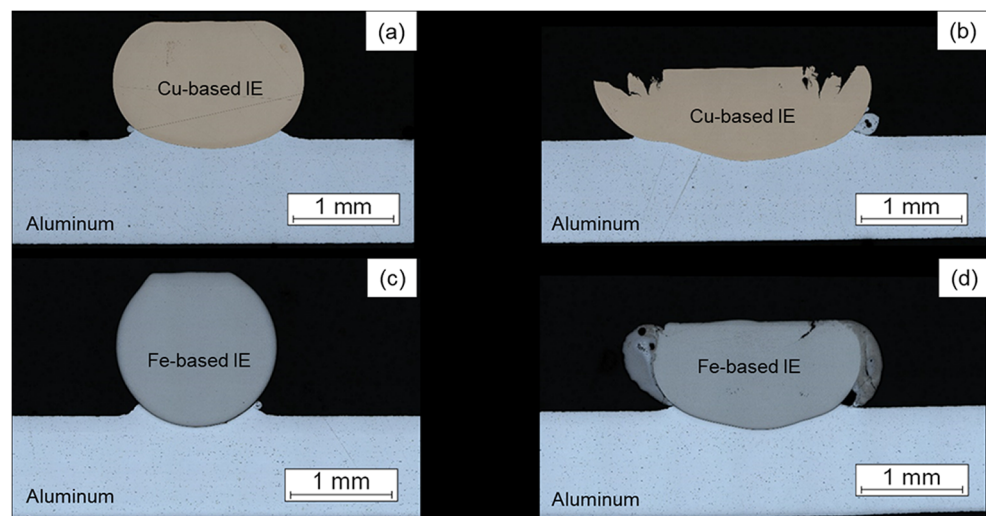
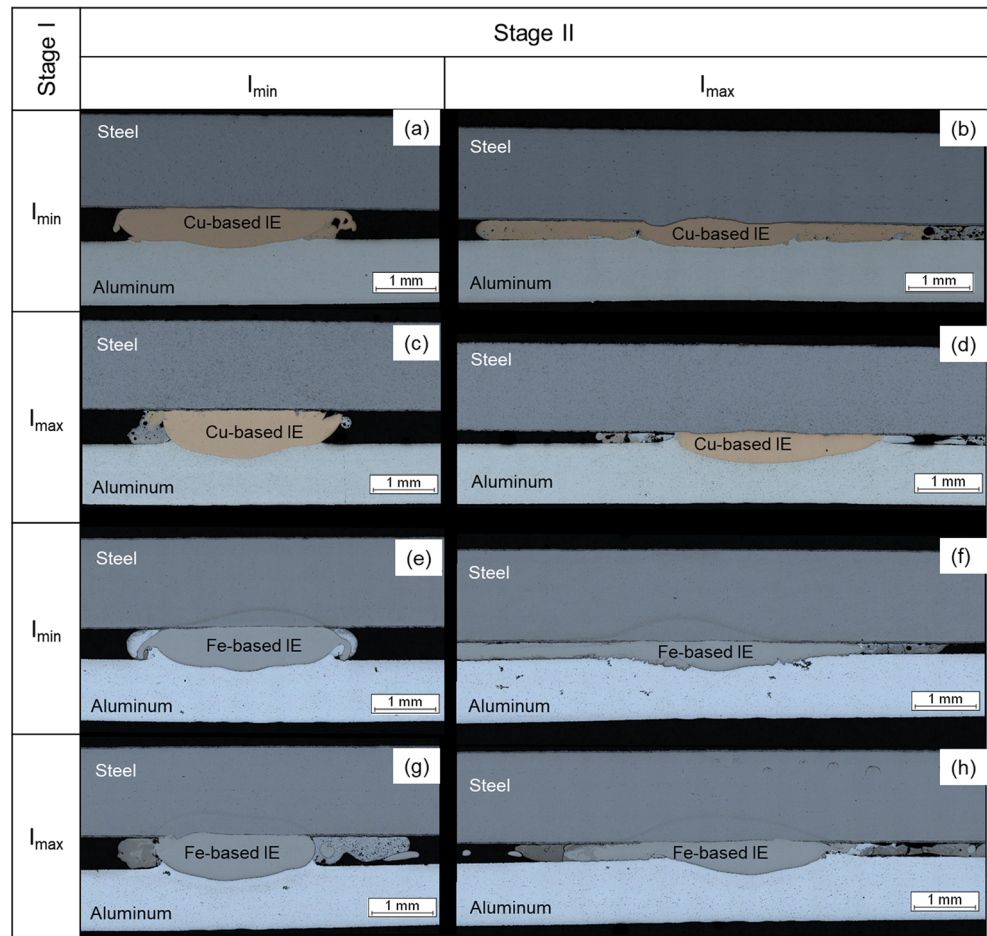


**Fig. 10** Cross sections of joints after stage II welded with 4 kN welding force and 16 ms welding time with **a, c, e, g** lower limit for welding current  $I_{\min}$  and **b, d, f, h** upper limit for welding current  $I_{\max}$  by using Cu-based and Fe-based insert elements (IE); **a, b, e, f** were welded with  $I_{\min}$  on the first stage, **c, d, g, h** with  $I_{\max}$  on the first stage



and upper limits with 2 kN and 10 ms using Cu-based and Fe-based insert elements. Increasing welding current leads to higher heat input and as a result stronger deformation of insert elements and larger connection area between aluminum and insert elements.

The cross section of an entire joint with element between steel and aluminum sheets is presented in Fig. 10 a–h. Joints (a), (b) with copper insert elements (IE), and (e) and (f) with steel insert elements were prepared using electrode force of 2 kN, 10 ms welding time, and lower limit for welding current

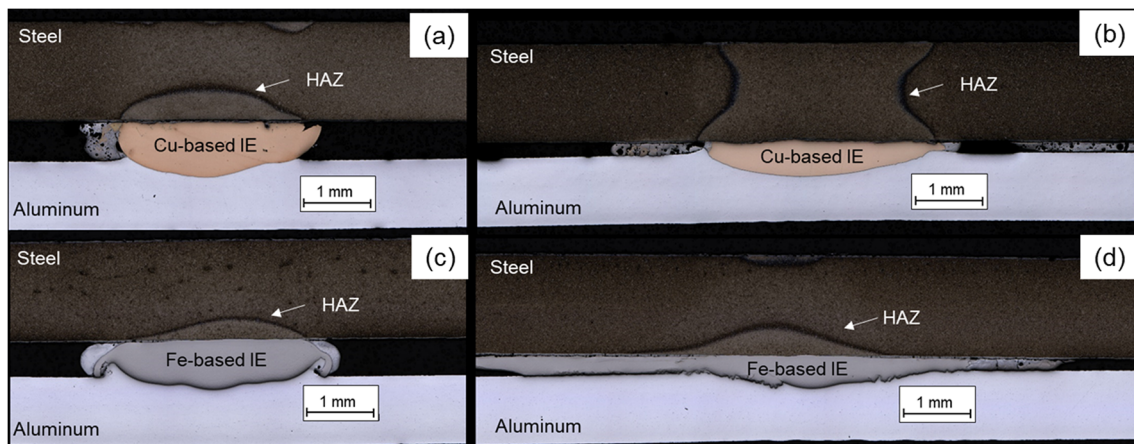


**Fig. 11** Cross sections of joints after stage II (nital-etched) welded with 4 kN welding force and 16 ms welding time with **a, c** lower limit for welding current and **b, d** upper limit for welding current by using Cu-based and Fe-based insert elements (IE)



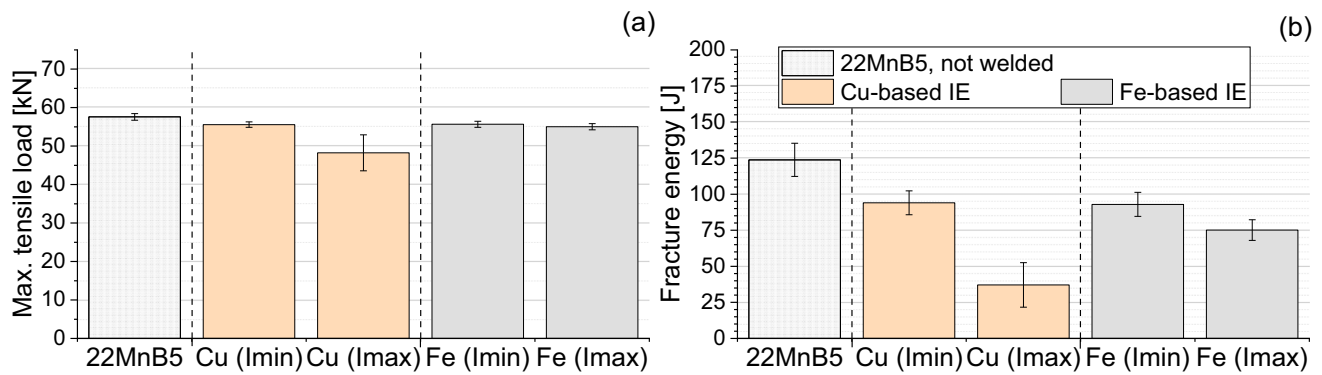


**Fig. 12** Maximum tensile load (a) and fracture energy (b) for 22MnB5 with one-sided loading with and without welds for two types of insert elements

( $I_{\min}$ ), and joints (c), (d), (g), and (h) with upper limit for welding current ( $I_{\max}$ ) on stage I. All presented joints were prepared using 4 kN welding force, 16 ms welding time on stage II, with a different welding current: joints (a), (c), (e), and (g) were welded with  $I_{\min}$  and (b), (d), (f), and (h) with  $I_{\max}$ .

Apparently, no nugget was formed in the joining plane. Increase of welding current led to greater plastic deformation of insert elements and, as result, to higher tensile shear strength due to larger joint surface. The insert elements in joints welded with lower limit for welding current ( $I_{\min}$ ) are less deformed, than that welded with upper limit for welding current ( $I_{\max}$ ). On the other hand, it is hard to find pronounced differences in joints welded with different welding current on stage I ( $I_{\min}$  and  $I_{\max}$ ).

Additionally, same cross sections after nital etching are presented in Fig. 11. Compared with unetched samples, the heat-affected zone in steel sheet can be observed. For both copper and steel insert elements with increase in welding current, the heat-affected zone grows. However, the joints with insert elements made of copper have more pronounced HAZ, due the higher welding current settings.

Assessment of the influence of heat-affected zone was made by tensile test of steel sheet with welded insert element and aluminum sheet. The results are shown in Fig. 12.

A slight drop in the maximum load values for specimens welded with insert elements in comparison with the base steel sheets can be observed. The maximum reduction of tensile load value can be observed in the samples welded with copper insert element with maximum welding current, which can be confirmed by the micrograph (Fig. 11 b). This tendency can be seen even better on the diagrams with fracture energy. When the welding current increases, the fracture energy decreases. That happens because of bigger heat-affected zone and the softening problem in the heat-affected zone. It is important to compare these results with conventional welding processes, where the welding time is longer and the heat-affected zone is bigger.

## 4 Conclusions

Investigations of a novel process for manufacturing aluminum to steel joints by projection welding with the use of insert elements by a stage welding process with a common MFDC welding machine was investigated. A method of defining the weldability lobe for joints without weld nugget, based on joint strength and geometry, was suggested.

It can be conducted that:

- (1) Chemical composition and geometry of insert elements can be widely varied due to a simple element manufacturing process, using commercially available welding wires.
- (2) Chemical composition and thus electrical properties of the insert elements have great influence on the position and size of the welding current range. Generally, much higher welding currents were needed to join more conductive copper-based elements, compared with resistive steel elements.
- (3) Welding current ranges of the investigated joining process are large, so that high process stability and good industrial usability of the process can be expected.
- (4) Further investigations of the process, including mechanical properties of the joints as well as metallurgical phenomena for short-time welding with high energy concentration, such as formation of intermetallics between Fe, Al, and Cu, must be conducted prior to industrial application of the process.

**Acknowledgments** The authors would like to thank AiF for funding the IGF-Project IGF-No. 20164 BR/FOSTA P1294 of the German Research Association for Steel Application (FOSTA), which was part of the program to support cooperative industrial research (Industrielle Gemeinschaftsförderung (IGF)) by the Federal Ministry for Economic Affairs and Energy, following a decision of the German Bundestag. Equal thanks go to all companies, colleagues, and students who contributed their support, knowledge, and effort to the project.

## References

- Hörhold R, Müller M, Merklein M, Meschut G (2016) Mechanical properties of an innovative shear-clinching technology for ultra-high-strength steel and aluminium in lightweight car body structures. In: *Welding in the World* 60(3):613–620. <https://doi.org/10.1007/s40194-016-0313-0>
- Jank N, Staufer H, Bruckner J (2008) Heft 5) Schweißverbindungen von Stahl mit Aluminium – eine Perspektive für die Zukunft. In: *BHM* 153:189–192. <https://doi.org/10.1007/s00501-008-0373-6>
- Ma Y, Lou M, Li Y, Lin Z (2018) Effect of rivet and die on self-piercing rivetability of AA6061-T6 and mild steel CR4 of different gauges. In: *Journal of Materials Processing Technology* 251:282–294. <https://doi.org/10.1016/j.jmatprotec.2017.08.020>
- Meschut G, Hahn O, Janzen V, Olfemann T (2014) Innovative joining technologies for multi-material structures. In: *Welding in the World* 58(1):65–75. <https://doi.org/10.1007/s40194-013-0098-3>
- Ueda K, Ogura T, Nishiuchi S, Miyamoto K, Nanbu T, Hirose A (2011) Effects of Zn-based alloys coating on mechanical properties and interfacial microstructures of steel/aluminum alloy dissimilar metals joints using resistance spot. In: *Materials Transactions Vol 52(5):967–973*. <https://doi.org/10.2320/matertrans.L-MZ201108>
- Miyamoto K, Nakagawa S, Sugi C, Sakurai H, Hirose A (2009) Dissimilar joining of aluminum alloy and steel by resistance spot welding. In: *SAE Int J Mater Manuf Vol 2:1*. <https://doi.org/10.1016/j.matdes.2019.107585>
- Friedrich HE (2013) Leichtbau in der Fahrzeugtechnik. Wiesbaden
- Hendrawan MA, Purboputro PI (2018) Influence of zinc on mechanical behavior of resistance spot welding of aluminum and stainless-steel. In: *AIP Conference Proceedings:S. 30048*. <https://doi.org/10.1063/1.5042968>
- Oikawa, H.; Ohmiya, S.; Yoshimura, T.; Saitoh, T.: Resistance spot welding of steel and aluminium sheet using insert metal sheet. In: *Science and Technology of Welding and Joining (1999) Vol. 4, No. 2*. <https://doi.org/10.1179/136217199101537608>
- Heiko R, Yang Y, Broda T, Koltschote C (2013) Neuartige Widerstandspunktschweißverfahren für den automobilen Aluminium-Stahl-Mischbau. Duisburg
- Zvorykina, A.; Holtschke, N.; Hübner, A.; Jüttner, S.: Manufacturing of steel-aluminum joints using combination of ultrasonic and resistance spot welding (in German). Untersuchungen zur Herstellung von Stahl-Aluminium-Verbindungen durch das kombinierte Ultraschall- und Widerstandspunktschweißen. Leipzig 2016
- Lu Y, Mayton E, Song H, Kimchi M, Zhang W (2019) Dissimilar metal joining of aluminum to steel by ultrasonic plus resistance spot welding - microstructure and mechanical properties. In: *Materials & Design* 165:S. 107585. <https://doi.org/10.1016/j.matdes.2019.107585>
- Meschut G, Janzen V, Olfemann T (2014) Innovative and highly productive joining technologies for multi-material lightweight car body structures. In: *Journal of Materials Engineering and Performance* 23(5):1515–1523. <https://doi.org/10.1007/s11665-014-0962-3>
- Holtschke N, Jüttner S (2017) Joining lightweight components by short-time resistance spot welding. In: *Welding in the World* 61(2): 413–421. <https://doi.org/10.1007/s40194-016-0398-5>
- Habenicht, G.: Kleben. Grundlagen, Technologien, Anwendungen, 6., aktualisierte Aufl. Berlin, Heidelberg 2009
- Kuhlmann, M.; Wohner, M.; Mitzschke, N.: Einfluss von Prozessbedingungen beim Formhärten auf die Verbindungseigenschaften gefügter Bauteile. In: Merklein, M.; Warmblechumformung, E. W. (Hrsg.): 12. Erlanger Workshop Warmblechumformung. Tagungsband zum 12. Erlanger Workshop Warmblechumformung : Erlangen, den 23. November 2017. Bamberg 2017
- Rusch, H.-J.; Stocks, N.: Vom Nutzen des Querdenkens. In: DVS - Deutscher Verband für Schweißen und verwandte Verfahren e.V., Düsseldorf (Hrsg.): 24. DVS-Sondertagung Widerstandsschweißen. Treffpunkt Widerstandsschweißen 2019
- Ketzel, M.-M.; Hertel, M.; Zschetzsche, J.; Füssel, U.: Heat development of the contact area during capacitor discharge welding. In: *Welding in the World* 50 (2019) 1, E2. <https://doi.org/10.1007/s40194-019-00744-x>
- Deutsches Institut für Normung e.V.: SEP1220-2: Prüf- und Dokumentationsrichtlinie für die Fügeignung von Feinblechen aus Stahl - Teil 2: Widerstandspunktschweißen (2011). Berlin
- Deutscher Verband für Schweißen und verwandte Verfahren e.V.: DVS 2911: Kondensatorentladungsschweißen - Grundlagen, Verfahren und Technik. (in German) (2016)

**Publisher's note** Springer Nature remains neutral with regard to jurisdictional claims in published maps and institutional affiliations.